Chinese Chemical Letters 35 (2024) 108565

Contents lists available at ScienceDirect

Chinese Chemical Letters

journal homepage: www.elsevier.com/locate/cclet

Modularized sulfur storage achieved by 100% space utilization host for high performance lithium-sulfur batteries

Jun Jiang[a], Tong Guo[a], Wuxin Bai[a], Mingliang Liu[a], Shujun Liu[a], Zhijie Qi[a], Jingwen Sun[a], Shugang Pan[b,*], Aleksandr L. Vasiliev[c], Zhiyuan Ma[a,d], Xin Wang[a], Junwu Zhu[a,*], Yongsheng Fu[a,*]

[a] Key Laboratory for Soft Chemistry and Functional Materials of Ministry of Education, Nanjing University of Science and Technology, Nanjing 210094, China
[b] Changzhou Institute of Technology, Changzhou 213032, China
[c] Shubnikov Institute of Crystallography, Russian Academy of Sciences, Leninskii pr. 59, Moscow 119333, Russia
[d] Jiangsu Pylon Battery Co., Ltd., Yangzhou 211400, China

ARTICLE INFO

Article history:
Received 3 March 2023
Revised 6 May 2023
Accepted 11 May 2023
Available online 12 May 2023

Keywords:
Modularized sulfur storage
Space utilization
Cathode host material
ZIF-67
Lithium-sulfur batteries

ABSTRACT

Popularization of lithium-sulfur batteries (LSBs) is still hindered by shuttle effect and volume expansion. Herein, a new modularized sulfur storage strategy is proposed to solve above problems and accomplished *via* employing 100% space utilization host material of cobalt loaded carbon nanoparticles derived from ZIF-67. The modular dispersed storage of sulfur not only greatly increases the proportion of active sulfur, but also inhibits the occurrence of volume expansion. Meanwhile, 100% space utilization host material can greatly improve the conductivity of the cathode, provide a larger electrolyte wetting interface and effectively suppress the shuttle effect. Moreover, loaded cobalt particles have high catalytic activity for electrochemical reaction and can effectively improve the redox kinetics. The cell with new cathode host material carbonized at 650 °C (ZIF-67 (650 °C)) exhibits superior rate performance and can maintain a high specific capacity of 950 mAh/g after 100 cycles at 0.2 C, showing a good cycle stability.

With the widespread application of new energy vehicles and large-capacity portable electronic devices, conventional lithium-ion batteries have been difficult to meet the requirements for the above emerging markets. Thus, it is very urgent to develop an effective substitute for lithium-ion batteries. Lithium-sulfur batteries (LSBs), with high energy density (2600 Wh/kg) and theoretical specific capacity (1675 mAh/g), unique advantages of rich sulfur resources, environment-friendly and low manufacturing cost [1–3], are widely regarded as one of the most potential commercial battery systems in the next generation.

However, at present, lithium-sulfur battery cannot be put into commercial use on a large scale because of some intractable scientific and technical problems: (1) The shuttle effect, caused by the high solubility of polysulfides and the intermediate product of electrode reaction dissolved in organic ether liquid electrolyte, makes the content of active substances involved in electrode reaction decrease and the interface deteriorate. The direct reaction between the intermediate products (such as Li_2S_8, Li_2S_6, Li_2S_4 and other polysulfides) and the anode lithium, seriously reduces the utilization rate of sulfur cathode and thus leads to rapid decline in capacity, low coulombic efficiency and battery failure. (2) The volume expansion/contraction, which is up to 79% during charge and discharge, causes the change of the morphology and structure of sulfur cathode, resulting in battery capacity attenuation and even battery damage. (3) The lithium dendrites, induced by inhomogeneous deposition of lithium ions, can not only reduce the coulombic efficiency, but also pierce the separator, leading to the internal short circuit and even combustion explosion of the battery.

It has been demonstrated that the ingenious construction of sulfur cathode multifunctional host materials with strong interaction and efficient catalytic conversion for polysulfides is expected to suppress the shuttle effect from the source as well as provide buffer space to accommodate the volume expansion/contraction and thus improve the actual energy density and service life of the battery [4–7]. Carbon-based nanomaterials have been widely used as sulfur cathode host materials due to good mechanical stability, excellent electrical conductivity, high natural abundance and large specific surface area [8]. Their excellent electrical conductivity can quickly conduct charge. Meanwhile, the large specific surface area has a strong adsorption effect on sulfur and polysulfides, facilitat-

* Corresponding authors.
E-mail addresses: pansg@czu.cn (S. Pan), zhujw@njust.edu.cn (J. Zhu), fuyongsheng@njust.edu.cn (Y. Fu).

https://doi.org/10.1016/j.cclet.2023.108565
1001-8417/

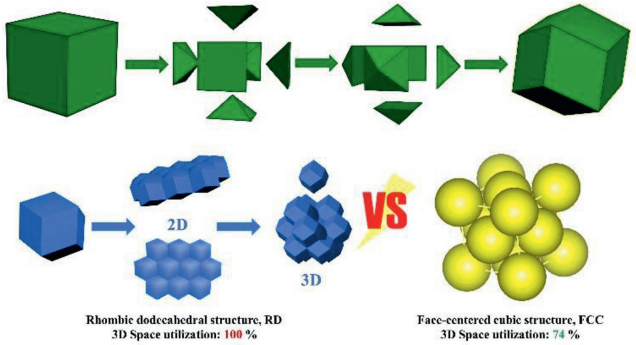

Fig. 1. Space utilization diagram of rhombic dodecahedron and sphere structure.

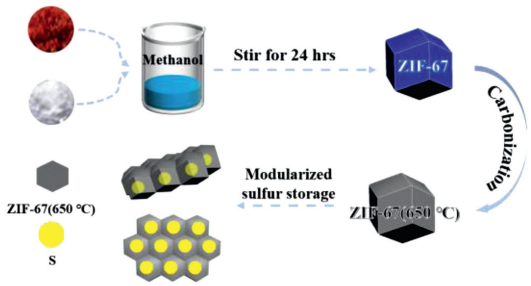

Fig. 2. The preparation of cathode composite.

ing to load more sulfur. Also, the nanostructures can limit polysulfides to the carbon matrix, thereby inhibit the occurrence of shuttle effect [9]. So far, many different shapes of carbon-based nanomaterials have been reported to be used as cathode host materials for LSBs, such as sphere [10], rods [11], sheets [12]. However, relatively little attention has been paid to the space utilization and the ability to increase the active sulfur content of these materials. Taking the spherical host materials as an example, according to the Kepler conjecture (proved by Thomas C. Hales [13]):

$$st = \oint_{a}^{b} \frac{\sin x}{x},\ b - a = n\ (n = dimension) \tag{1}$$

the maximum space utilization rate of sphere structure is 74% ($n = 3$) (Fig. 1). Particles are mostly in point-point contacting, leading to the small reaction area and less reaction active sites. The loose accumulation also causes the problem that the shuttle effect will still occur when some sulfur escapes from a single host particle. Therefore, the shape of the cathode host materials must be considered to achieve maximum space utilization and more effectively suppress the shuttle effect.

ZIF-67, prepared from the complexation and self-assembly of 2-methylimidazole and Co^{2+} [14], has large specific surface area, adjustable pore size [15] and most importantly, its rhombic dodecahedron structure enables tightest stacking for 100% space utilization (Fig. 1). In recent years, many researchers have found that MOFs materials can be used as precursors to prepare carbon-supported transition metal compounds by carbonization treatment, which can not only retain the original structure and morphology, but also enhance the interaction between carbon support and catalyst [16–18]. During carbonization treatment, ZIF-67's original three-dimensional crystal framework will shrink inward but still maintain a rhombic dodecahedron structure, therefore, it is expected to be used as a prefect sulfur host material [19].

In this work, a new modularized sulfur storage strategy is proposed and accomplished *via* employing 100% space utilization host material of cobalt loaded carbon nanoparticles derived from ZIF-67. The modularized sulfur storage strategy can not only effectively suppress the shuttle effect and volume expansion, but also increase the active sites of sulfur participating in reaction. More importantly, unlike most spherical cathode host materials, the as-obtained cobalt loaded carbon nanoparticles inherit unique rhombic dodecahedron structure of ZIF-67, which can theoretically achieve 100% space utilization. When the host particles are tightly packed, surface-to-surface contact can greatly improve the conductivity of the cathode and provide a larger electrolyte wetting interface. Moreover, when sulfur escapes from a single host particle, it will still enter another one, thereby avoiding the loss of active sulfur. Also, parallel experiments confirm that the sample carbonized at 650 °C has the best effect of storing sulfur. As a result, the assembled Li–S battery delivers a high discharge capacity of 950 mAh/g and the capacity retention rate is up to 84% after 100 cycles at 0.2 C, which is significantly better than lithium-sulfur batteries assembled with other different shapes of host materials.

Cobalt nitrate hexahydrate and 2-methylimidazole were used as raw materials to prepare the precursor ZIF-67 (Fig. 2). The nitrogen atoms at the 1,3 positions of the imidazole rings will release protons to cooperate with Co^{2+}, thereby forming an extended three-dimensional crystal network structure with a periodic arrangement of metal node-imidazole ring-metal node as the monomer (Fig. S1 in Supporting information) [20]. The SEM image of ZIF-67 precursor is shown in Fig. S2a (Supporting information). It can be seen that ZIF-67 precursor has a typical rhombic dodecahedron structure and the width and height of ZIF-67 crystal are both about 0.5 μm [21]. Also, because the size of ZIF-67 particles is at the nanometer level, most of the particles are clustered together [22]. The X-ray diffraction (XRD) and Raman spectroscopy were applied to verify the crystallographic structure and chemical compositions. The XRD pattern of ZIF-67 is in good agreement with the simulated crystal pattern, indicative of a significant crystallinity (Fig. S2b in Supporting information). In Raman spectrum (Fig. S2c in Supporting information), the stretching vibration peaks of Co-N, C-N and C-C bonds are observed at 265, 685 and 1455 cm^{-1} [23]. ZIF-67 precursor possesses a high BET specific surface area of 1200 m^2/g and abundant mesoporous and micropores (Fig. S2d in Supporting information).

ZIF-67 precursor was further used to prepare cobalt loaded carbon nanoparticles cathode host material by one-step heat treatment method. During the carbonization process of ZIF-67, NH_3 and H_2 are generated by ligand decomposition of ZIF-67, which can reduce Co^{2+} to metal cobalt particles with high catalytic activity for the electrochemical reaction of the cells, and thus effectively improving the redox kinetics [24]. Meanwhile, organic ligand residues will be further converted into N-doped carbon on Co particles under Co particles catalysis. As-obtained ZIF-67 (500 °C), ZIF-67 (650 °C) and ZIF-67 (800 °C) samples still retained the original rhombic dodecahedron structure of ZIF-67 (Figs. 3a, d and g). However, after sulfur loading treatment, ZIF-67 (500 °C) and ZIF-67 (800 °C) are entirely wrapped with sulfur (Figs. 3b, c, e and f), implying a failed sulfur storage. But surprisingly, for ZIF-67(650 °C), nearly all the sulfur is encapsulated successfully and there is no visible sulfur on the surface (Figs. 3h-i). The EDS mappings (Figs. 3j-m) and TGA curve (Fig. S3 in Supporting information) were employed to confirm the successful storage of sulfur in ZIF-67 (650 °C). As shown in Fig. S3, all sulfur was triumphantly stored in ZIF-67 (650 °C), which proves the excellent sulfur storage capacity of this host material.

The XRD patterns and the Raman spectra of carbonized products are shown in Fig. 4a and Fig. S4a (Supporting information). The intensity of peaks at 44° and 52° attributed to metal Co increases with the enhanced carbonization temperature, indicating that Co^{2+} has been reduced to Co (JCPDS card No. 15–0816) dur-

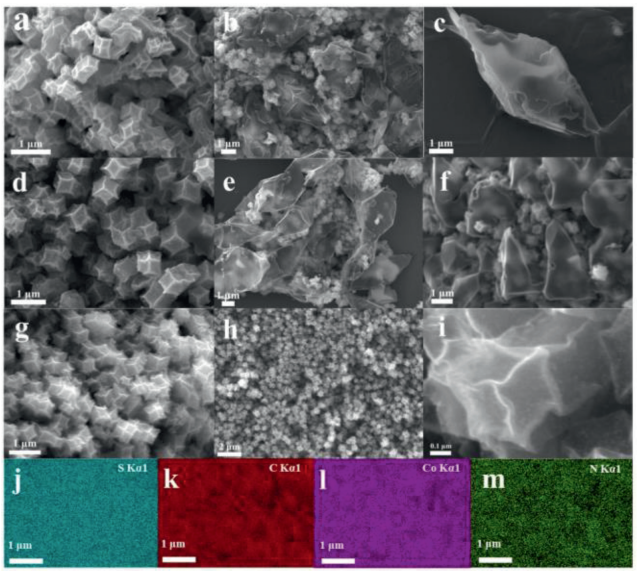

Fig. 3. SEM of samples carbonized at (a) 500 °C, (d) 800 °C, (g) 650 °C, (b, c) S@ZIF-67 (500 °C), (e, f) S@ZIF-67 (800 °C), (h, i) S@ZIF-67 (650 °C). EDS image of S@ZIF-67 (650 °C): (j) S, (k) C, (l) Co, (m) N (corresponding to Fig. 3h).

ing carbonization process. The cobalt catalyst can be expected to accelerate the transformation of polysulfides, inhibit the shuttle effect and thus improve cell performance [25]. After sulfur loading treatment, the XRD patterns (Fig. 4b) and the Raman spectra (Fig. S4b in Supporting information) display characteristic peaks of sulfur, further demonstrated that the sulfur have already been loaded in the ZIF-67 (650 °C).

The BET specific surface area and pore size distribution of ZIF-67 (650 °C) both of before and after sulfur loading were tested as contrast (Fig. 4c). It can be seen that ZIF-67 (650 °C) has a high BET specific surface area of (290 m^2/g) with abundant mesoporous and micropores. After sulfur loading treatment, the BET specific surface area of S@ZIF-67 (650 °C) dramatically decreases from 290 m^2/g to 3 m^2/g. Meanwhile, all the mesoporous and micropores also disappear (Fig. S5 in Supporting information). This may be ascribed to the fact that all the sulfur are encapsulated in ZIF-67 (650 °C) *via* capillary condensation. Moreover, the large specific surface area and rich pore structure of ZIF-67 (650 °C) can be used to anchor polysulfides through physical limitation and chemical adsorption.

With copious N-doped structures, ZIF-67 (650 °C) has strong chemical adsorption capacity for LPSs and can efficiently inhibit the shuttle of LPSs and enhance stability of LSBs. Adsorption experiments of Li_2S_6 solutions (2 mmol/L) were carried out in parallel to visually explore the trapping effect of the carbonized samples toward polysulfides. In general, the adsorption of LPSs is correlated with the BET surface area of the adsorbent. However, even though the precursor's BET surface area is 4 times as large as the carbonized samples, the adsorption effect of the latter is much better than the former. As shown in Fig. 4d, the color of Li_2S_6 solution was initially dark yellow and its color strength decreased to varying degrees along with the adding of different carbonized products, among which the effect of ZIF-67 (650 °C) is the most significant, whose color has already been vitreous and clear after immersion for 6 h. The ultraviolet (UV) spectrum was utilized to further explore the degree of adsorption toward LPSs (Fig. 4d). Predictably ZIF-67 (650 °C) showed the weakest LPSs adsorption peaks, indicating its best adsorption capacity toward LPSs [26].

XPS measurements were performed to help us better evaluate the strong chemical interactions between ZIF-67 (650 °C) and LPSs. Figs. 4e and f exhibit the high-resolution N 1s and Co 2p XPS spectra of ZIF-67 (650 °C) before and after the Li_2S_6 adsorption test, respectively. After interacting with Li_2S_6, the N 1s and Co 2p peaks significantly shift to lower binding energy while the S 2p peaks shift to higher binding energy (Fig. S6 in Supporting information), which denotes the electron transfer from S to N and Co to form strong chemical interaction. Also, a new Co-S peak (779.2 eV) appeared after ZIF-67 (650 °C) interacts with Li_2S_6, indicating Co and S atoms have been bonded as well [27,28].

The anchoring effects of ZIF-67 (650 °C) for polysulfides can be quantified by calculating the binding energy between polysulfides and substrates. Herein, the binding energies of S_8 and Li_2S_n (n = 1, 2, 4, 6 and 8) with graphitic N, pyrrolic N and pyridinic N, which has been detected in XPS measurements have been displayed in Figs. 5a and b and Fig. S7 (Supporting information). The binding energies of Li_2S, Li_2S_2, Li_2S_4, Li_2S_6 and Li_2S_8 on pyridinic N reaches 2.63, 2.75, 2.32, 2.04 and 2.45 eV, respectively. With regards to the pyrrolic N, the binding energies are 2.10, 2.51, 2.17, 1.95 and 2.16 eV, respectively, indicating the rich pyridinic N and pyrrolic N structures of ZIF-67 (650 °C) have high binding strength for poly-

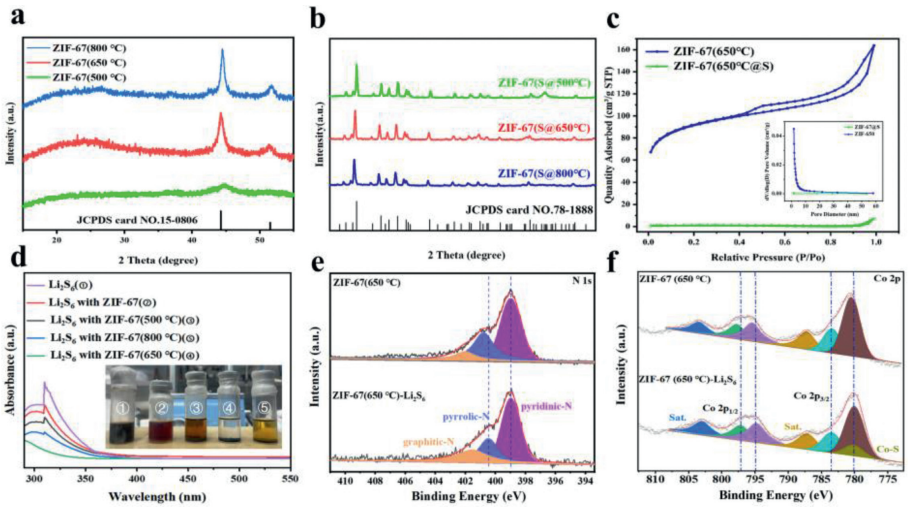

Fig. 4. XRD patterns of (a) carbonized samples and (b) carbonized samples@S. (c) N_2 adsorption/desorption isothermal linear plots and pore size distribution of ZIF-67 (650 °C) before/after sulfur loading. (d) Static adsorption test of Li_2S_6 on different materials and UV−vis spectra with corresponding photos of Li_2S_6 solution before and after adsorption test. (e, f) High-resolution N 1s and Co 2p XPS spectra of the ZIF-67 (650 °C) and ZIF-67 (650 °C) after adsorption test of Li_2S_6.

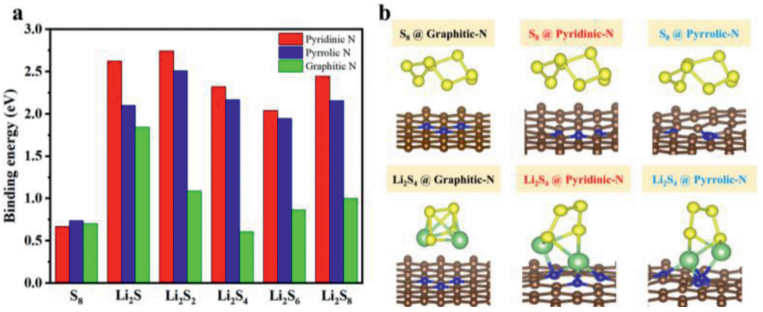

Fig. 5. (a) Binding energy between Li_2S_n, S_8 and pyridinic N, pyrrolic N and graphitic N. (b) Adsorption model of Li_2S_4, S_8 with pyridinic N, pyrrolic N and graphitic N.

sulfides. Therefore, as cathode host material, ZIF-67 (650 °C) can effectively capture polysulfides, thus inhibiting the occurrence of shuttle effect.

To deeply figure out the effect of carbonized samples in inhibiting the shuttle of polysulfides, *in-situ* Raman spectroscopy was conducted to help us achieve a better comprehension of the reaction mechanism of LSBs by detecting the Raman signal of polysulfides shuttling to the anode in real-time (The test conditions are detailed in Supporting information) [29]. The discharge process of LSBs assembled with ZIF-67 (800 °C) is shown in Fig. S8 (Supporting information), during the preliminary stage (>2.30 V), three distinct characteristic peaks appeared at 152, 218 and 473 cm^{-1}, which should be respectively attributed to the bending and stretching vibration of S_8^{2-} [30,31]. Besides that, a Raman signal of S_6^{2-} is also detected at 399 cm^{-1}. Proceeded to discharge to 2.30 V, S_8^{2-} gradually transforms into S_6^{2-}, thus the intensity of characteristic peaks of S_8^{2-} and S_6^{2-} significantly decrease and increase. However, along with the conversion, the shuttle effect becomes more severe as well. With the discharge going on, two peaks with gradually enhanced intensity of S_4^{2-} are observed at 200 and 448 cm^{-1}, which indicates that sustained shuttle effect should also be partly attributed to S_4^{2-}. As for the charge procedure, the shuttle effect is equally severe as well (Fig. S9 in Supporting information). Therefore, in this cell, the serious shuttle effect caused by LPSs (mainly S_6^{2-} and S_4^{2-}) occurs throughout the whole battery reaction process, leading to nonreversible loss of sulfur. Contrarily, for the LSBs assembled with ZIF-67 (650 °C), during the discharge (Figs. 6a and b) and charge (Fig. S10 in Supporting information) process, peaks of S_4^{2-} surprisingly disappeared and the intensity of S_6^{2-} characteristic peaks was also greatly weaken, indicating that LPSs have been firmly fixed on the cathode and the shuttle effect was effectively pressed by ZIF-67 (650 °C). Above results can powerfully demonstrate that ZIF-67 (650 °C) effectively suppresses the shuttle effect of LPSs through the synergistic effect of abundant chemisorption sites and strong physical adsorption.

In-situ XRD technique was conducted to directly supervise the evolution of polysulfide and reveal how the carbonized samples inhibit shuttle effect (The test conditions are detailed in Supporting information). The result of the cell with ZIF-67 (650 °C) as cathode host material is shown in Fig. 6c, the characteristic peaks at about 22.6° are assigned to the α-S_8 [32,33]. As the discharge proceeds, the intensities of S_8 peaks continuously decrease. When the discharge process came to the second discharge stage B, a new characteristic peak with gradually enhanced intensity of crystalline cubic Li_2S appears at the very beginning of the lower-discharge plateau, indicating the continuous formation of Li_2S. Afterwards, the intensities of Li_2S peak continuously increase and eventually reach the maximum value. Oppositely, oxidation of various sulfur species occurs during charge, mainly reflecting in the decrease of Li_2S yield (stage D) and generation of new characteristic peaks, which represent the formation of monoclinic β-S_8 [33,34].

Compared with the cell with ZIF-67 (650 °C) as cathode host material, for the cell with ZIF-67 (800 °C) as cathode host material, the peak intensity (Fig. S11 in Supporting information) of Li_2S is much weaker and there are fewer characteristic peaks of β-S_8 after the charge is completed, proving that the shuttle effect in this cell is more severe. Therefore, due to its excellent ability to effectively store sulfur inside, the performance of the cell with ZIF-67 (650 °C) as cathode host material is obviously better.

To estimate carbonized samples' ability to inhibit shuttle of LPSs, the shuttle currents of LSBs with different cathode host materials were recorded. The concentration of LPSs reaches a maximum at a potential of 2.38 V during the charge/discharge process, resulting in a maximum shuttle current [35,36]. As shown in Fig. 7a, the cell with ZIF-67 (650 °C) as cathode host material shows the lowest shuttle current (0.035 mA), almost negligible. This result also shows ZIF-67 (650 °C)'s outstanding trapping capacity for LPSs and ability to inhibit the diffusion of LPSs to the anode electrode.

To verify the electrocatalytic properties of carbonized samples toward the polysulfide conversion, the cyclic voltammetry (CV) test of Li_2S_6-Li_2S_6 symmetric cells was conducted in the voltage range of -1.0∼1.0 V. As shown in Fig. 7b, the symmetrical cell with ZIF-67 (650 °C) as cathode host material shows a higher redox current and smaller polarization at a scan rate of 6 mV/s, which demonstrates faster LPSs redox kinetics [37,38].

The electrochemical impedance spectroscopy (EIS) spectra of the cells with different cathode host materials are shown in Fig. 7c with an equivalent circuit model inset, which shows the equivalent circuit. The R_{ct} of the cell with ZIF-67 (650 °C) as cathode host material (45.84 Ω) is much smaller than that of other two cells ((ZIF-67 (800 °C) ∼62.15 Ω and (ZIF-67 (500 °C) ∼147.8 Ω), indicating higher lithium-ion diffusivity and excellent effect in accelerating the ion/electron transfer to the active sites at the cathode interface. This result can be attributed to the outstanding ability of ZIF-67 (650 °C) in decreasing the interface resistance and accelerating the charge transport.

To further investigate the role of carbonized samples in the liquid-solid conversion of LPSs, Li_2S nucleation and growth test were also carried out. The potentiostatic discharging curves of Li_2S precipitation at 2.05 V based on different electrode materials (carbon paper matrix coated by different carbonized samples) are presented in Figs. 7d-f and the capacity was calculated based on the mass of sulfur in electrolyte. Obviously, the responsivity of Li_2S nucleation for the cell with ZIF-67 (650 °C) as cathode host material is earlier than that of other two cells, suggestive of a relatively faster kinetics of the liquid-solid conversion [39,40]. Moreover, the nucleation capacity ($Li_2S_4 \rightarrow Li_2S$) on ZIF-67 (650 °C) (621.79 mAh/g) is much larger than that on ZIF-67 (500 °C) (429.69 mAh/g) and ZIF-67 (800 °C) (528.7 mAh/g) even within a shorter nucleation and growth time, further revealing that the effective deposition of Li_2S is induced by ZIF-67 (650 °C) catalyst [41].

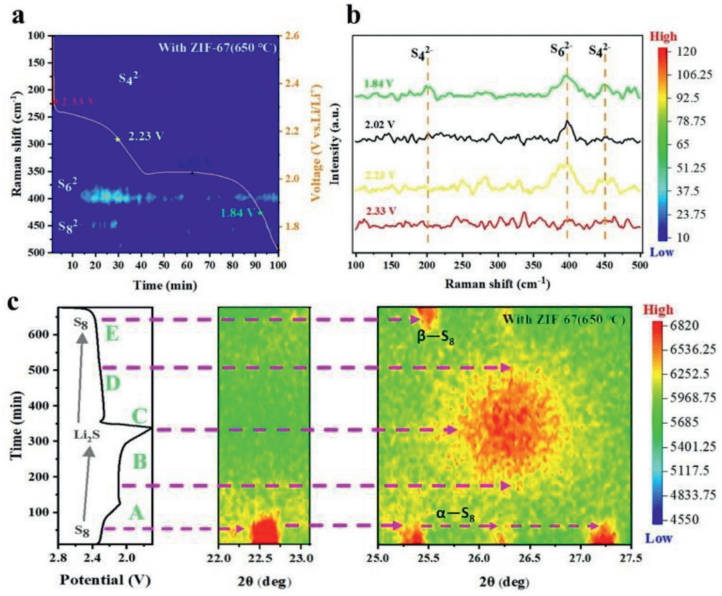

Fig. 6. (a, b) *In-situ* time-resolved Raman spectra and selected Raman spectra of Li-S cell with ZIF-67 (650 °C) as cathode host material (the aurantia curves represent the discharging processes). (c) *In-situ* XRD characterization in contour plots of Li-S cell with ZIF-67 (650 °C) as cathode host material and corresponding change-discharge profiles.

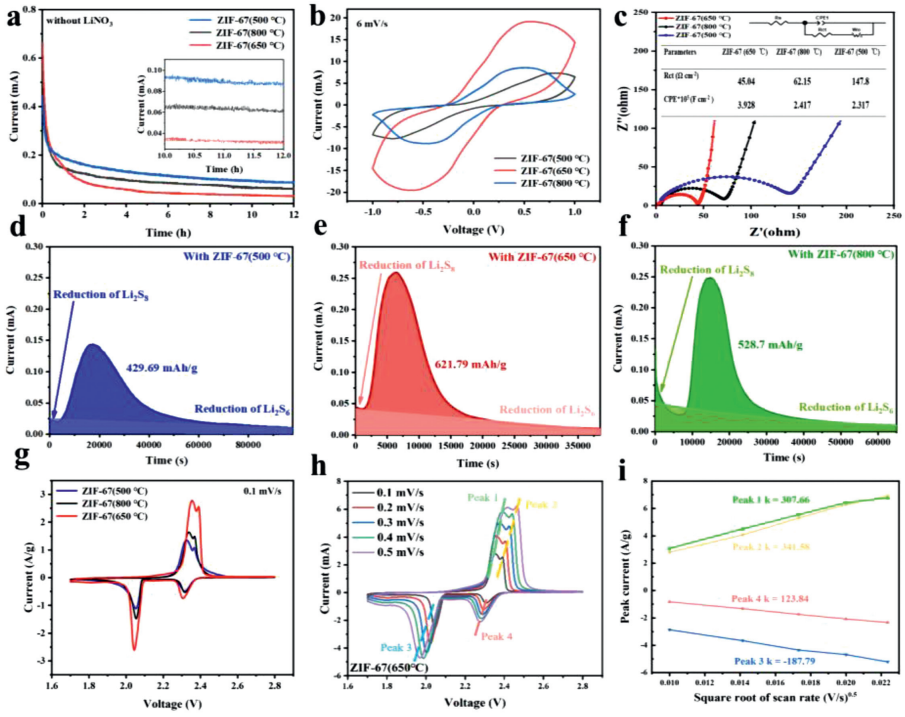

Fig. 7. (a) The shuttle currents of LSBs with different cathode host materials. (b) CV curves of Li_2S_6 symmetric cells with different electrodes. (c) The electrochemical impedance spectroscopy spectra of the cells with different cathode host materials. (d-f) Potentiostatic discharge plots of cells with different cathode host materials at 2.05 V. (g) CV profiles of Li-S cells with different cathode host materials at a scan rate of 0.1 mV/s. (h, i) CV curves and relationships between peak current and scan rate of cell with ZIF-67 (650 °C) as cathode host material at different scan rates respectively.

Fig. 7g presents the CV profiles of the Li-S coin cells with different cathode host materials in the voltage window of 1.7-2.8 V under a scan rate of 0.1 mV/s [42–44]. It should be noted that the cell with ZIF-67 (650 °C) as cathode host material exhibits the largest current signals and the lowest reaction polarization (Fig. S12 in Supporting information) for all redox peaks, indicating a significantly reinforced sulfur redox kinetics. This should be attributed to the synergistic effect between the modularized cathode host materials and cobalt particles. The surface-to-surface contact between the modularized carbonized materials greatly improves the conductivity of the cathode composite. At the same time, the rich N-doped structure and Co particles can improve the bidirectional conversion of polysulfides.

CV curves of LSBs with ZIF-67 (650 °C) as cathode host material and the corresponding relationships between peak current and scan rate are shown in Fig. 7h. The linear relationship indicates that this step is mainly controlled by the diffusion process of LPSs [45–47]. The Li-ion diffusion capability can be described by

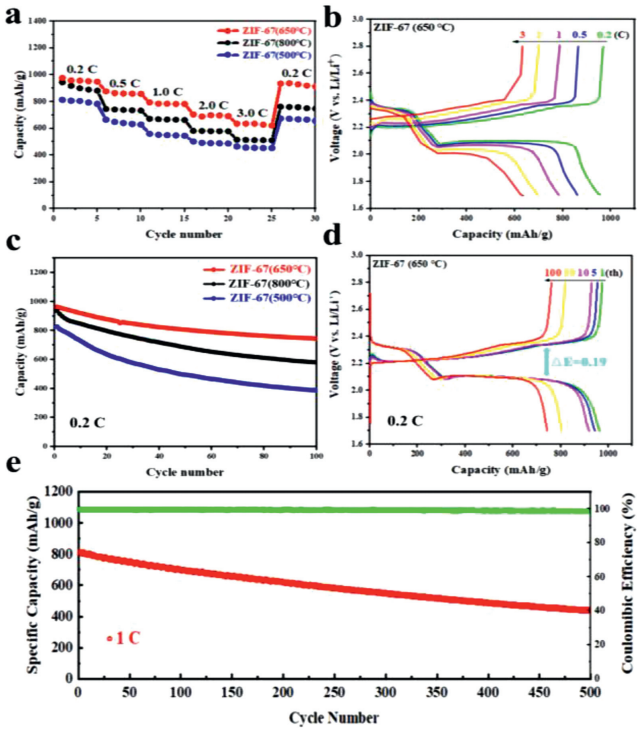

Fig. 8. (a) Rate performance of cells with different cathode host materials at different specific current. (b) Galvanostatic charge-discharge profiles of cell with ZIF-67 (650 °C) as cathode host material under different C-rates. (c) Cycling performance of cells with different cathode host materials at 0.2 C. (d) Galvanostatic charge-discharge profiles of cell with ZIF-67 (650 °C) as cathode host material at 0.2 C. (e) Long-term cycling stability of cell with ZIF-67 (650 °C) as cathode host material at 1 C.

the Randles–Sevick equation [48,49]:

$$I_p = \left(2.69 \times 10^5 \right) \times n^{1.5} \times AD^{0.5} \times Cv^{0.5} \ (25\ ^\circ C) \quad (2)$$

I_p represents the theoretical peak current, n is the number of charge transfers during the reaction, A is the area of the active electrode, D is the lithium-ion diffusion coefficient, C is the concentration of lithium-ion and v is the scan rate. The slope of plots not only stands for the diffusion rate of lithium ions but also indicates the diffusivity of sulfide species. As shown in Fig. 7i, the slopes of the oxidation peaks (peak 1 and peak 2) are both above 300 and the slopes of the reduction peaks (peak 3 and peak 4) are also above 120, indicating that the diffusion rate of LPSs in the electrode reaction is very fast, which proves that ZIF-67 (650 °C) can realize fast diffusion process. This new cathode host material has a strong adsorption capacity for polysulfides and can be used as an effective electrocatalyst to accelerate the diffusion and transformation kinetics of intermediate LPSs and inhibit the shuttle of LPSs. In addition, the modularized structure can provide sufficient reactive sites to catalyze the diffusion conversion of LPSs as well.

Rate performances of cells with different cathode host materials were evaluated at 5 different current densities from 0.2 C to 3.0 C (Fig. 8a). Unsurprisingly the cell with ZIF-67 (650 °C) as cathode host material achieves the highest specific discharge capacities of 990, 900, 800, 750 and 720 mAh/g at 0.2, 0.5, 1.0, 2.0 and 3.0 C, respectively. When the current density is restored to 0.2 C, the cell with ZIF-67 (650 °C) as cathode host material still possesses the capacity of 960 mAh/g, demonstrating the high stability and fast reaction kinetics. The corresponding galvanostatic charge-discharge (GCD) profiles are given in Fig. 8b and Fig. S13 (Supporting information). All the GCD curves exhibit two typical discharge plateaus and one charge plateau, which is consistent with the previous CV results and the multi-step sulfur reaction mechanism.

The cycling performance of cells with different cathode host materials are depicted in Fig. 8c, among which the cell with ZIF-67 (650 °C) as cathode host material manifests superior cycling performance. After 100 cycles at 0.2 C, the reversible capacity of 950 mAh/g with capacity retention of 84% can be maintained. In contrast, the cells with other two carbonized samples as cathode host materials show a significant capacity fading. After 100 cycles, the GCD curves still all exhibit two typical discharge plateaus and this cell has higher high-voltage plateau capacity (Q_H) and low-voltage plateau capacity (Q_L) (Fig. 8d and Fig. S14 in Supporting information), indicating its higher sulfur utilization and enhanced conversion kinetics [50]. Also, the lower polarization rate (ΔE) shows its better redox reaction kinetics [51,52]. The cell with ZIF-67 (650 °C) as cathode host material has higher initial capacity and lower capacity decay rate, indicating that the shuttle effect has been effectively suppressed and the loss of cathode active material in electrochemical reaction is less, which should be attributed to the tightly packed modularized structure.

Additionally, the long-term cycle test of the cell with ZIF-67 (650 °C) as cathode host material was further measured at 1 C (Fig. 8e), which exhibits the excellent cycling stability. The cell with ZIF-67 (650 °C) as cathode host material attains outstanding long cycle stability even at a large current density: A reversible discharge capacity of 450.3 mAh/g after 500 cycles at 1.0 C, high-capacity retention of 55.3% and a low-capacity fading rate of 0.089%. This new cathode host material successfully inhibits the occurrence of the shuttle effect and avoids the loss of active sulfur, thus improving capacity and cycle stability.

Lastly, we compared the performance of lithium-sulfur batteries assembled with a variety of cathode host materials in other shapes (Table S2 in Supporting information). As cathode host material, ZIF-67 (650 °C) can deliver better performance of lithium-sulfur batteries with less cathode mass ratio. This may be attributed to the fact that the ZIF-67 (650 °C) inherit unique rhombic dodecahedron structure of ZIF-67, which can theoretically achieve 100% space utilization (Fig. 1). When the host particles are tightly packed, surface-to-surface contact can greatly improve the conductivity of the cathode and provide a larger electrolyte wetting interface. Moreover, when sulfur escapes from a single host particle, it will still enter another one, thereby avoiding the loss of active sulfur, resulting in an excellent electrochemical performance.

In summary, a new modularized sulfur storage strategy is proposed and accomplished *via* employing 100% space utilization host material of cobalt loaded carbon nanoparticles derived from ZIF-67. Modularly dispersing sulfur can not only greatly increase the proportion of active sulfur, but also inhibit the shuttle effect and volume expansion, thereby improving the cycle stability of the LSBs. Moreover, due to the close accumulation of the rhombic dodecahedron structure, the surface-to-surface contact between the crystals also greatly enhances the conductivity of the cathode side. Cells assembled with ZIF-67 (650 °C) exhibit significantly better performance when compared with those assembled with other shapes of cathode host materials. Moreover, ZIF-67 (650 °C) possesses sufficient excellent conductivity, abundant Co particles and rich N-doped structures, which have high catalytic activity for electrochemical reaction and can effectively improve the redox kinetics. This work confirms the feasibility of modular dispersion treatment of sulfur and exhibits a new cathode host material for improving the performance of LSBs.

Declaration of competing interest

The authors declare that they have no known competing financial interests or personal relationships that could have appeared to influence the work reported in this paper.

Acknowledgments

This work was supported by the National Natural Science Foundation of China (No. 52173255), the Opening Project of the Jiangsu Key Laboratory for Chemistry of Low-Dimensional Materials (No. JSKC20021), and the Collaborative Innovation Center for Advanced Micro/nanomaterials and Equipment (Co-constructed by Jiangsu Province and Ministry of Education).

Supplementary materials

Supplementary material associated with this article can be found, in the online version, at doi:10.1016/j.cclet.2023.108565.

References

[1] P.G. Bruce, S.A. Freunberger, L.J. Hardwick, et al., Nat. Mater. 11 (2012) 19–29.
[2] J. Pu, Z. Shen, C. Zhong, et al., Adv. Mater. 32 (2020) 1903808.
[3] L. Zhou, D.L. Danilov, R.A. Eichel, Adv. Energy Mater. 11 (2020) 2001304.
[4] S. Liu, X. Hong, D. Wang, et al., Electrochim. Acta 279 (2018) 10–18.
[5] J. Cheong, C. Hu, W. Liu, et al., Nano Energy 102 (2022) 107659.
[6] F. Li, Y. Wu, Y. Lin, et al., J. Colloid. Interf. Sci. 626 (2022) 535–543.
[7] T. Xiao, Y. Yang, M. Yang, et al., J. Alloys Compd. 923 (2022) 166334.
[8] T. Zhang, C. Li, F. Wang, et al., Chem. Rec. 22 (2022) e202200083.
[9] X. Peng, Y. Lu, L. Zhou, et al., Nano Energy 32 (2017) 503–510.
[10] J. Wan, J. Wu, X. Gao, et al., Adv. Funct. Mater. 27 (2017) 1703933.
[11] C. Qi, S. Zu, X. Zhu, et al., Appl. Surf. Sci. 601 (2022) 154245.
[12] Z. Shi, R. Du, C. Yu, et al., J. Alloys. Compd. 925 (2022) 166642.
[13] T. Hales, M. Adams, G. Bauer, et al., Ann. Math 162 (2015) 1065–1185.
[14] M. Eddaoudi, J. Kim, N. Rosi, et al., Science 295 (2002) 469–472.
[15] Y. He, S. Hwang, D. Cullen, et al., Energy. Environ. Sci. 12 (2019) 250–260.
[16] Y. Qian, I.A. Khan, D. Zhao, Small 13 (2017) 1701143.
[17] L. Yang, X. Zeng, W. Wang, et al., Adv. Funct. Mater. 28 (2018) 1704537.
[18] Q. Wang, H. Zhao, B. Li, et al., Chin. Chem. Lett. 33 (2022) 4350–4356.
[19] L. Chen, C. Zheng, F. Cao, et al., J. Electron. Mater. 51 (2022) 4107–4114.
[20] H. Dai, W. Zhou, W. Wang, et al., J. Hazard. Mater. 426 (2022) 127784.
[21] H. Pan, X. Wang, H. Chu, et al., Opt. Lett. 44 (2019) 5892–5895.
[22] X. Zhang, F. Yan, X. Ma, et al., Adv. Energy. Mater. 11 (2021) 2102141.
[23] J. Meng, C. Niu, L. Xu, et al., J. Am. Chem. Soc. 139 (2017) 8212–8221.
[24] A. Wei, L. Wang, Y. Wang, Mater. Rep. 35 (2021) 13052–13057 13066.
[25] T.Y. Chen, L. Lin, D. Geng, et al., Electrochim. Acta 376 (2021) 137986.
[26] M. Wang, D. Yin, Y. Cao, et al., Chin. Chem. Lett. 32 (2021) 1157–1160.
[27] D. Deng, F. Xue, Y. Jia, et al., ACS Nano 11 (2017) 6031–6039.
[28] Y. Zhong, L. Yin, P. He, et al., J. Am. Chem. Soc. 140 (2018) 1455–1459.
[29] L. Xue, Y. Li, A. Hu, et al., Small Struct. 3 (2022) 2100170.
[30] W. Yao, W. Zheng, J. Xu, et al., ACS Nano 15 (2021) 7114–7130.
[31] J. Xia, W. Hua, L. Wang, et al., Adv. Funct. Mater. 31 (2021) 2101980.
[32] S. Walus, C. Barchasz, R. Bouchet, et al., Adv. Energy Mater. 5 (2015) 1500165.
[33] S. Yu, X. Huang, X. Schwarz, et al., Energy Environ. Sci. 11 (2018) 202–210.
[34] J. Conder, R. Bouchet, S. Trabesinger, et al., Nat. Energy. 2 (2017) 17069.
[35] Y. Fu, Z. Wu, Y. Yuan, et al., Nat. Commun. 11 (2020) 845.
[36] D. Moy, A. Manivannan, S.R. Narayanan, J. Electrochem. Soc. 162 (2015) A1–A7.
[37] J. Xu, W. Tang, C. Yang, et al., ACS Energy Lett. 6 (2021) 3053–3062.
[38] C. Wang, L. Sun, K. Li, et al., ACS Appl. Mater. Interfaces 12 (2020) 43560–43567.
[39] Z. Ye, Y. Jiang, L. Li, et al., Adv. Mater. 32 (2020) 2002168.
[40] M. Liu, P. Chen, X. Pan, et al., Adv. Funct. Mater. 32 (2022) 2205031.
[41] H. Yuan, H. Peng, B. Li, et al., Adv. Energy Mater. 9 (2019) 1802768.
[42] Y. Dong, D. Cai, T. Li, et al., ACS Nano 16 (2022) 6414–6425.
[43] Z. Shi, Z. Sun, J. Cai, et al., Adv. Mater. 33 (2021) 2103050.
[44] G. Jiang, N. Zheng, X. Chen, et al., Chem. Eng. J. 373 (2019) 1309–1318.
[45] Y. Liu, D. Han, L. Wang, et al., Adv. Energy Mater. 9 (2019) 1803477.
[46] J. He, A. Manthiram, Adv. Energy Mater. 10 (2020) 2002654.
[47] V. Augustyn, P. Simon, B. Dunn, Energy Environ. Sci. 7 (2014) 1597–1614.
[48] X. Tao, J. Wang, C. Liu, et al., Nat. Commun. 7 (2016) 11203.
[49] L. Ji, X. Wang, Y. Jia, et al., Adv. Funct. Mater. 30 (2020) 1910533.
[50] H. Shi, Z. Sun, W. Lv, et al., J. Energy Chem. 45 (2020) 135–141.
[51] Q. Xu, Y. Wang, X. Shi, et al., Green Chem. 23 (2021) 942–950.
[52] Z. Sun, S. Vijay, H.H. Heenen, et al., Adv. Energy. Mater. 10 (2020) 1904010.